Supporting information

Electrochemical oxidation of lignin model compounds over metal oxyhydroxides on nickel foam

Zhang Danlu, Zeng Xu, Wang Sinong, Xu Yan, Dai Qiqi, Yue Fengxia, Wang Peng, Liu Chuanfu, Lan Wu*

Content

Preparation of β–O–4 lignin dimer models

The β–O–4 lignin dimeric model compounds were prepared according to the reference [1]. The non-phenolic β–O–4 dimer model materials VG and TG were started with non-phenolic ketones. They are prepared by Bromination, Etherification, Aldol condensation and Carbonyl reduction.

Phenolic β–O–4 dimer models GG and SS were initiated by Benzylation of phenolic ketones to protect hydroxyl groups. Then Bromination, Etherification, Aldol condensation, Carbonyl reduction and debenzyl Debenzylation were carried out successively.

The synthesis routes of different lignin β–O–4 dimer models are as follows.

Fig. S1 The synthetic route of VG.

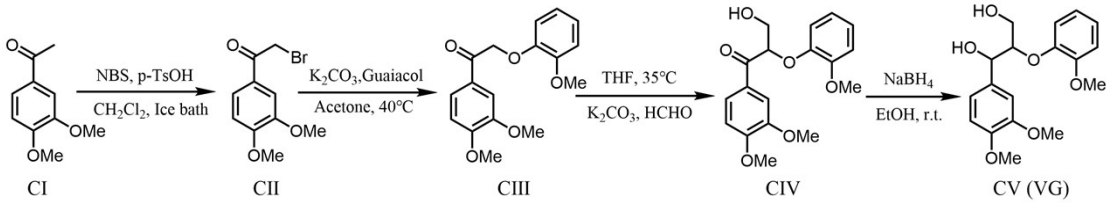

Fig. S2 The synthetic route of TG.

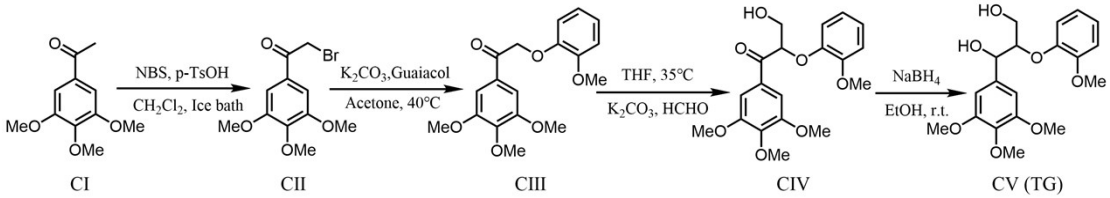

Fig. S3 The synthetic route of GG.

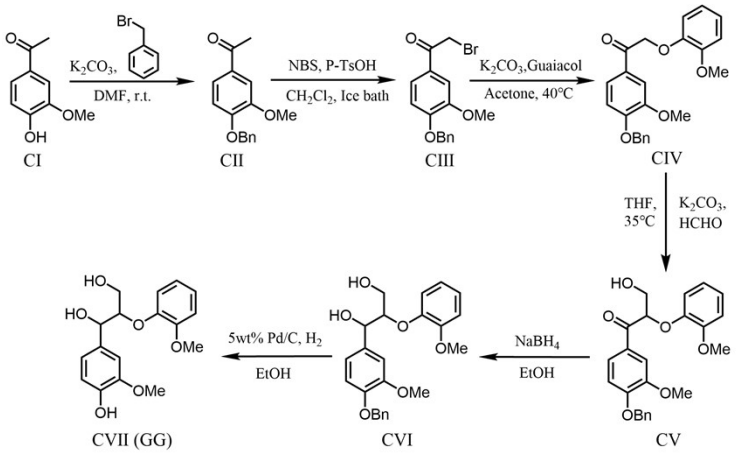

Fig. S4 The synthetic route of SS.

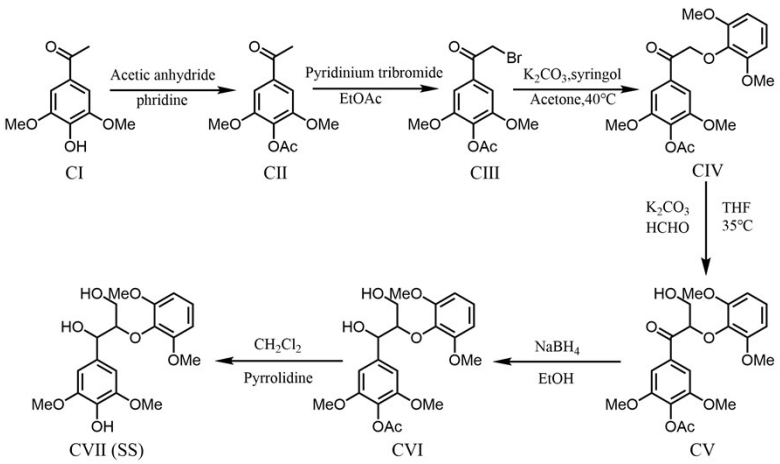

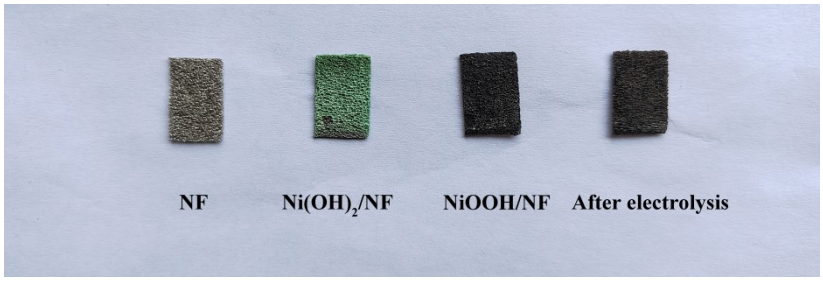

Fig. S5 A digital photo of NF, $Ni(OH)_2$/NF and NOOH/NF before and after nine hours of electrolysis.

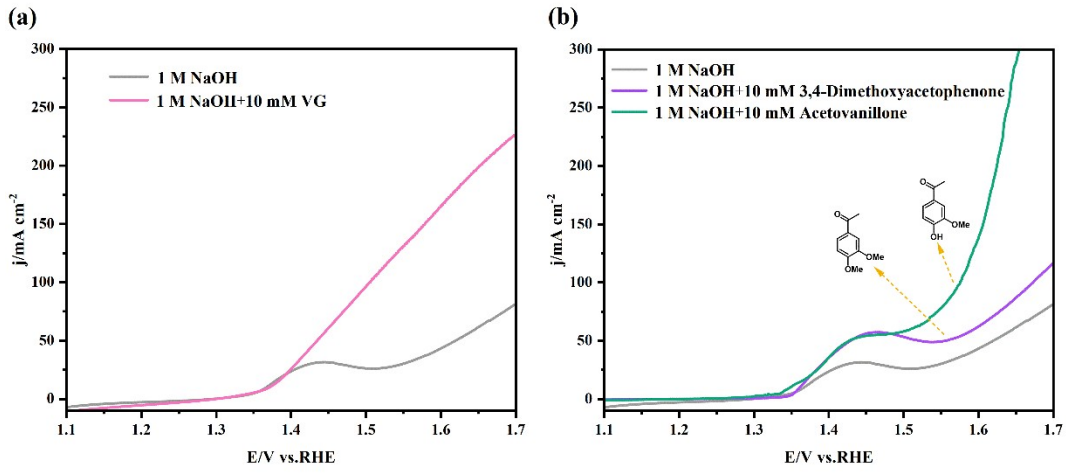

Fig. S6 LSV curve of NiOOH/NF in 1 M NaOH solution with (a) 10 mM VG, (b) 10 mM 3,4-dimethoxyacetophenone and 10 mM acetovanillone.

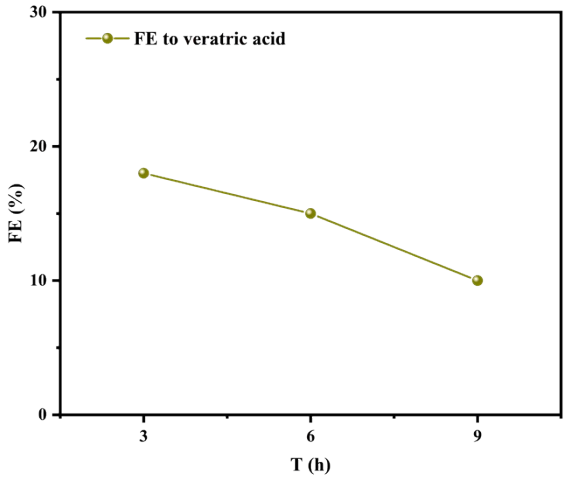

Fig. S7 Faradic efficiency (FE) to veratric acid as the function of reaction time.（Suppose the first reaction path of Fig. 8 is followed，the number of transferred electrons is 8）

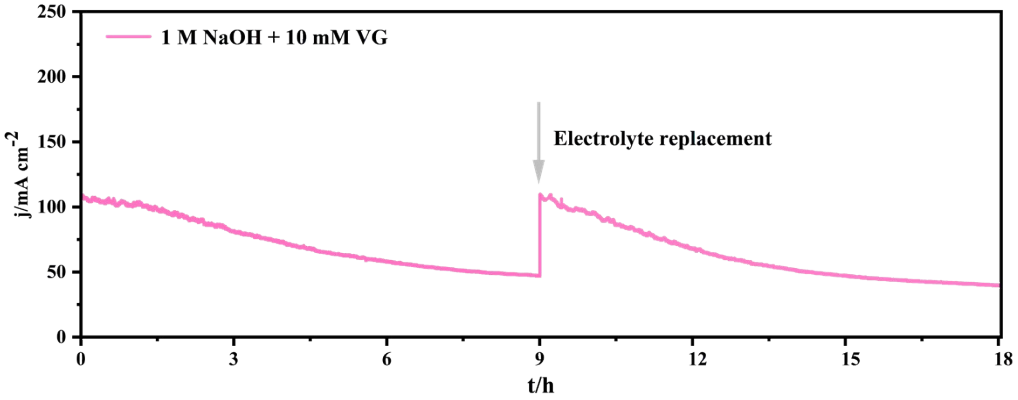

Fig. S8 i-t curves of NiOOH/NF for VG (10mM in 1 M NaOH) oxidation at 1.6 V.

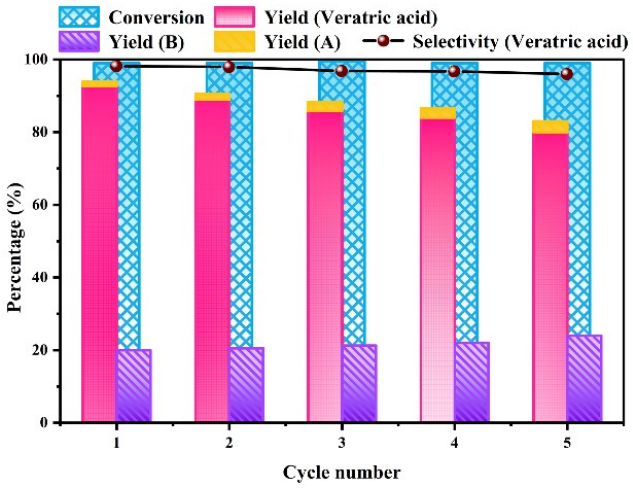

Fig. S9 Catalyst cyclability test.

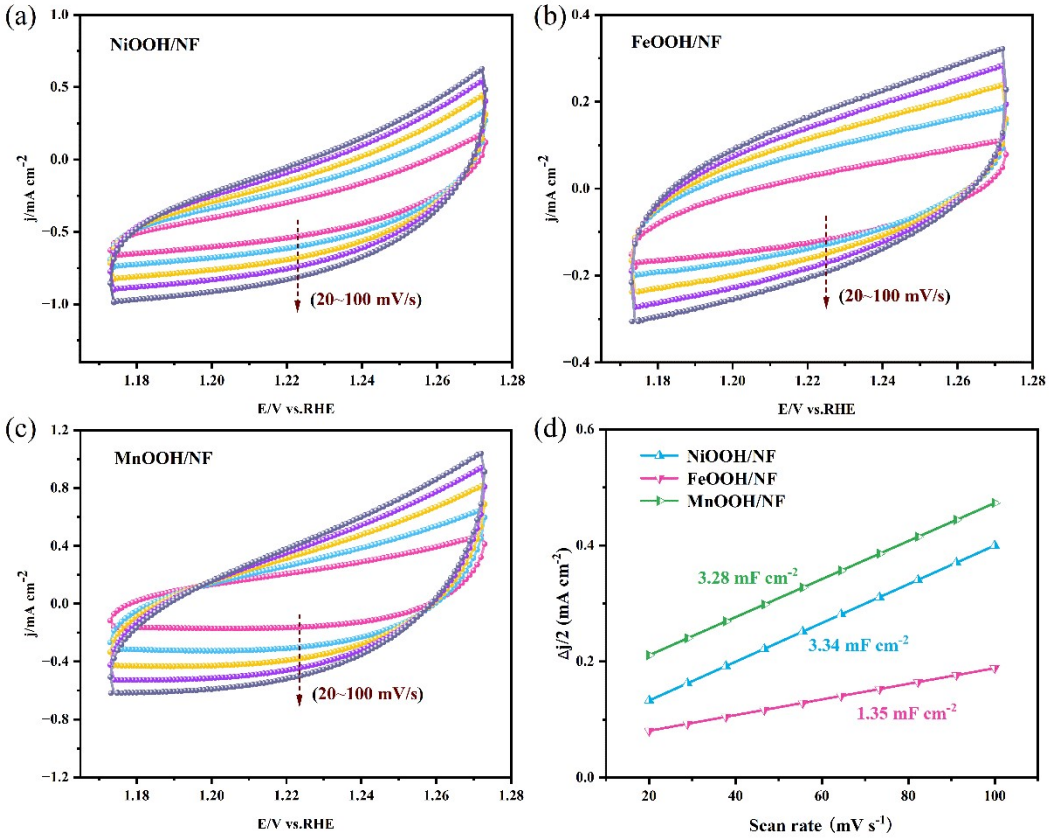

Fig. S10 (a-c) CV cycle curves at different scanning rates. (d) The calculated double-layer capacitance (Cdl).

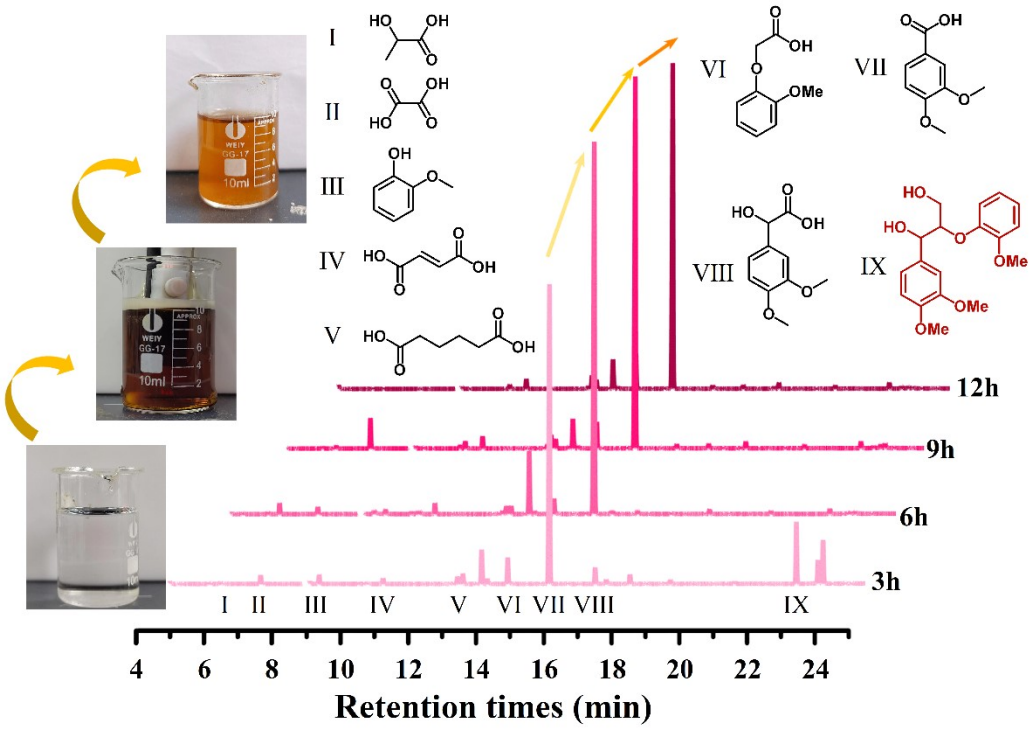

Fig. S11 GCMS chromatograms of the products after electrocatalytic oxidation of VG and the color of the solution changes during electrolysis.

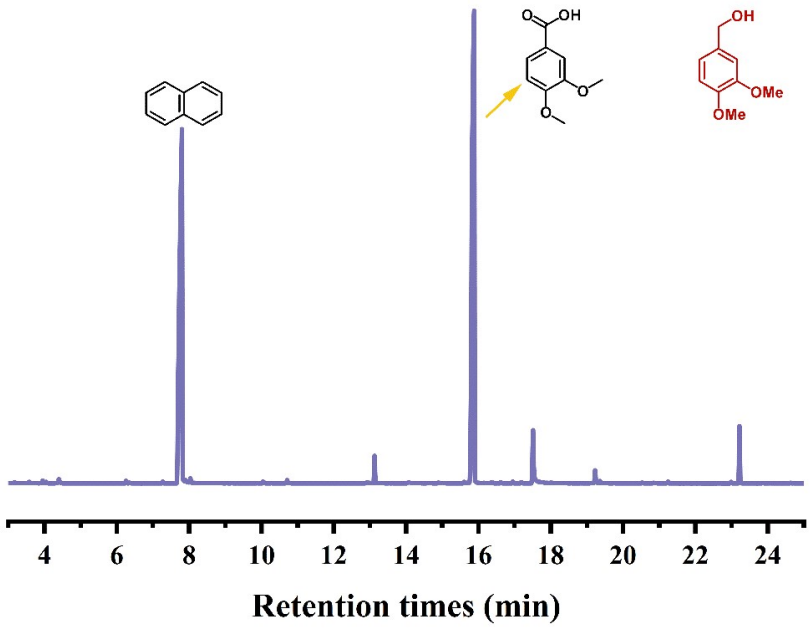

Fig. S12 GCMS chromatogram of the products after electrocatalytic oxidation of veratryl alcohol.

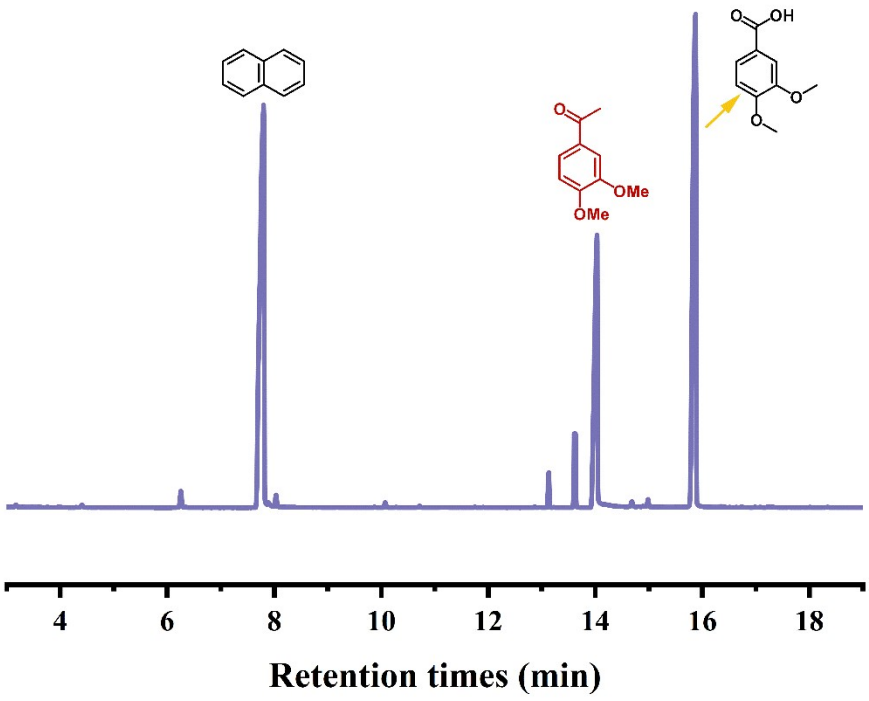

Fig. S13 GCMS chromatogram of the products after electrocatalytic oxidation of 3,4-dimethoxyacetophenone.

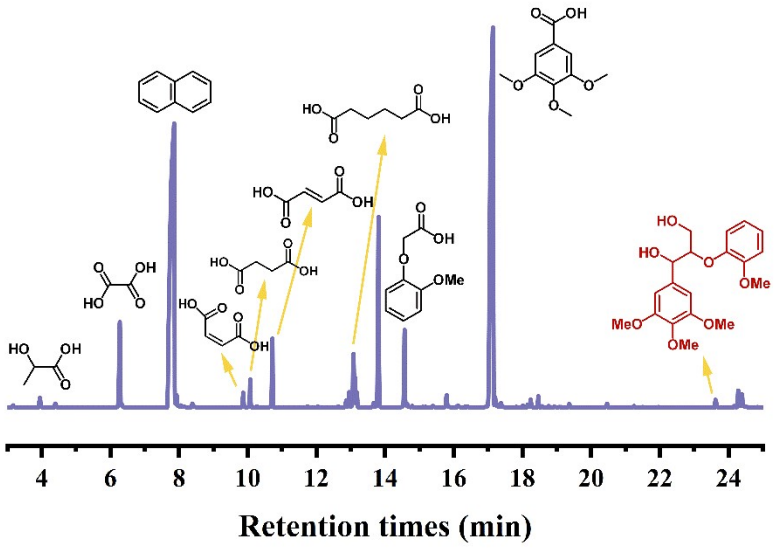

Fig. S14 GCMS chromatogram of the products after electrocatalytic oxidation of TG.

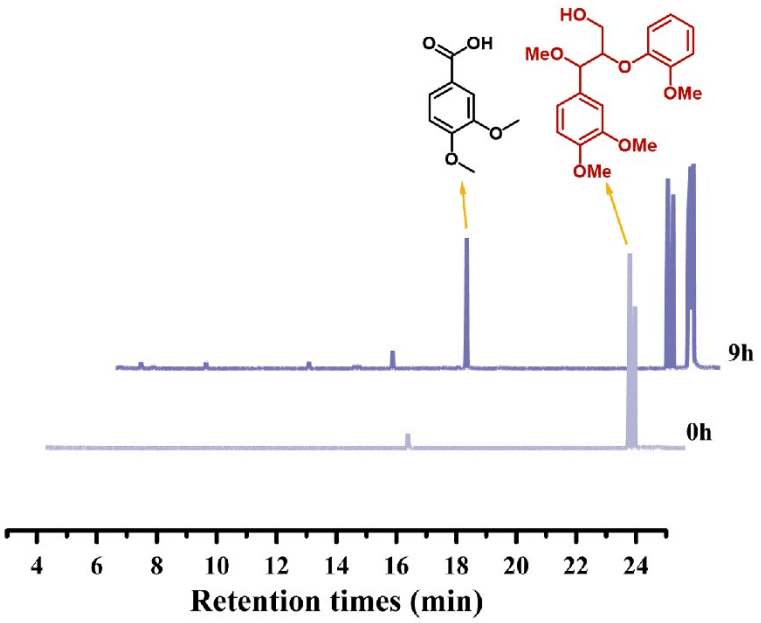

Fig. S15 GCMS chromatogram of the products after electrocatalytic oxidation of α-methylated VG.

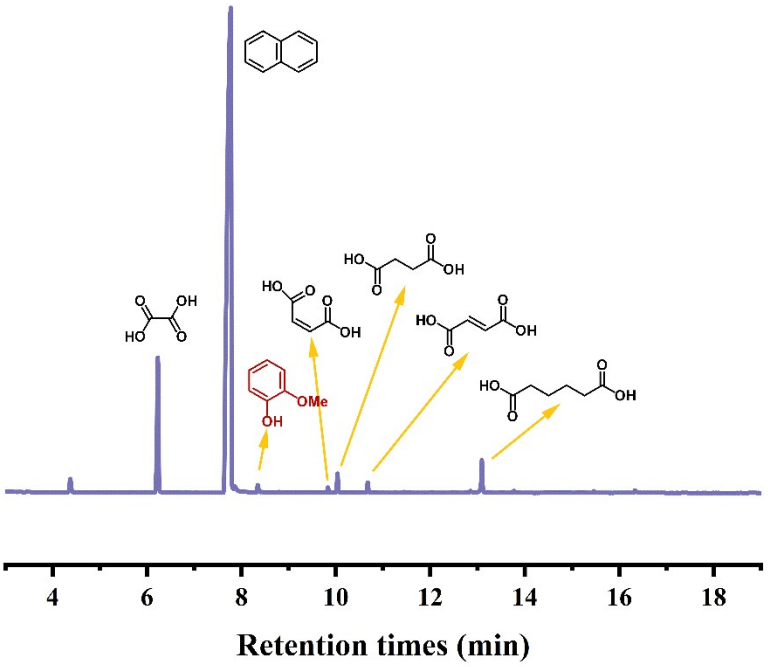

Fig. S16 GCMS chromatogram of the products after electrocatalytic oxidation of guaiacol.

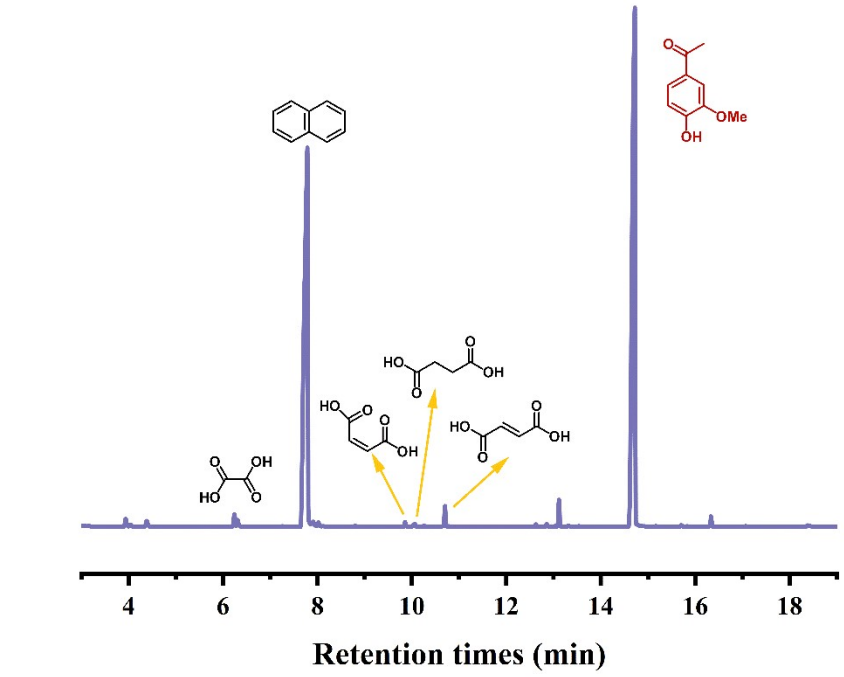

Fig. S17 GCMS chromatogram of the products after electrocatalytic oxidation of acetovanillone.

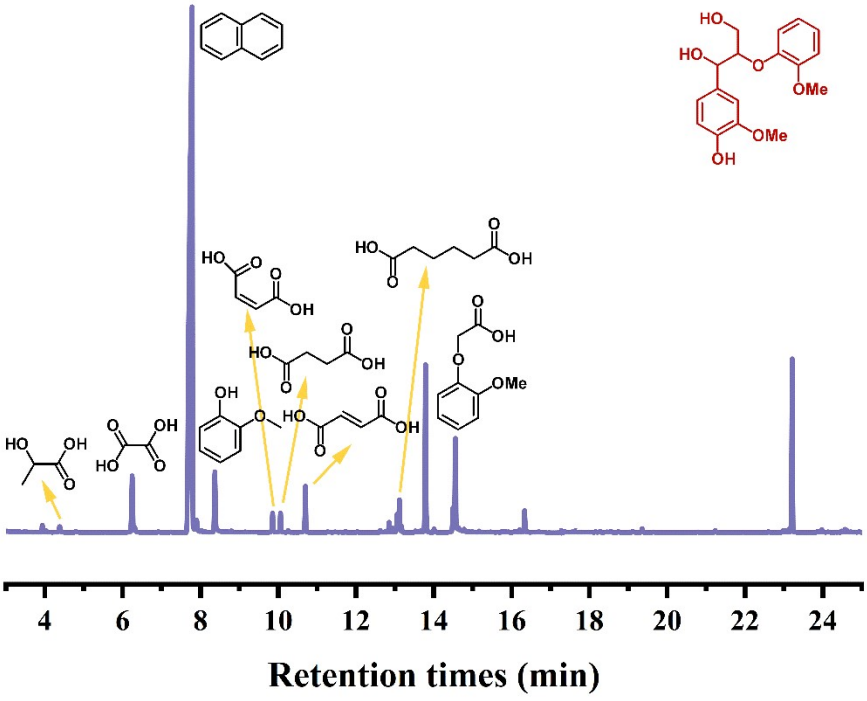

Fig. S18 GCMS chromatogram of the products after electrocatalytic oxidation of GG.

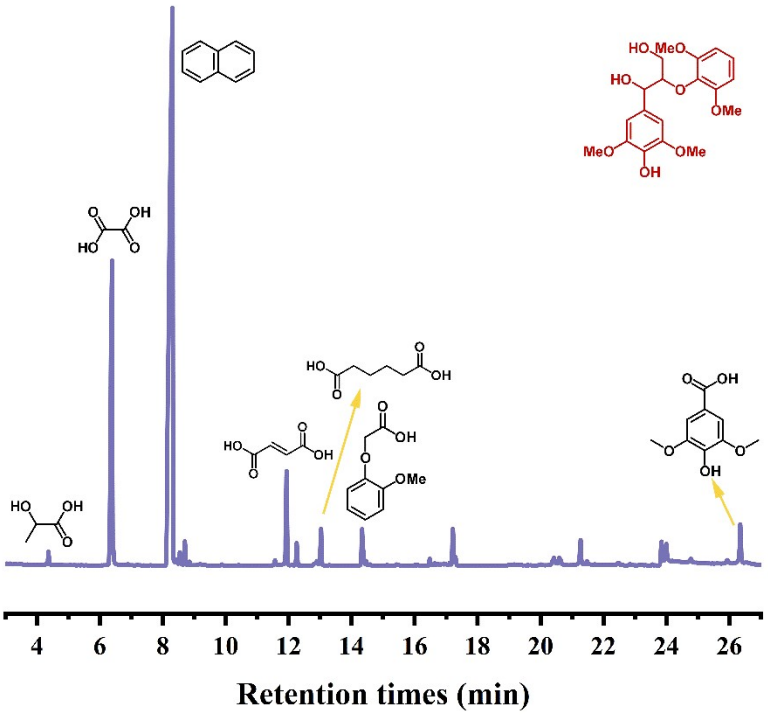

Fig. S19 GCMS chromatogram of the products after electrocatalytic oxidation of SS.

Fig. S20 Mass spectrograms of all products.

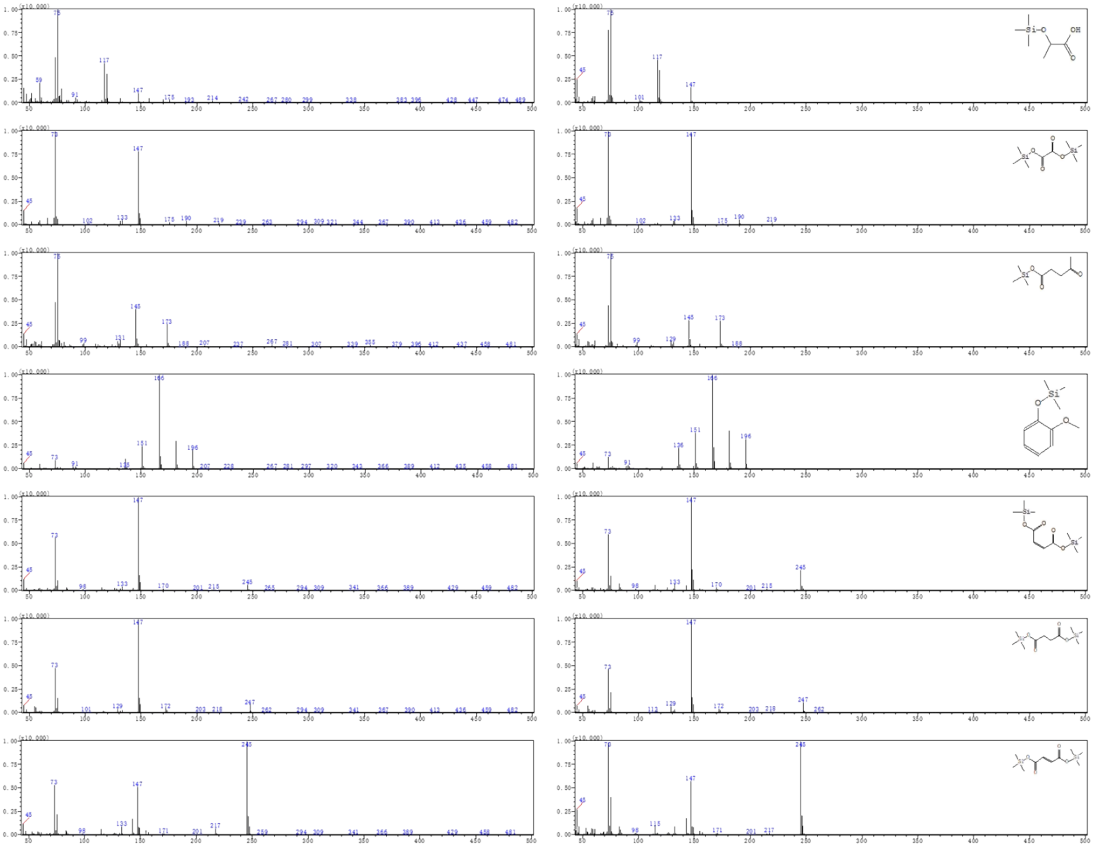

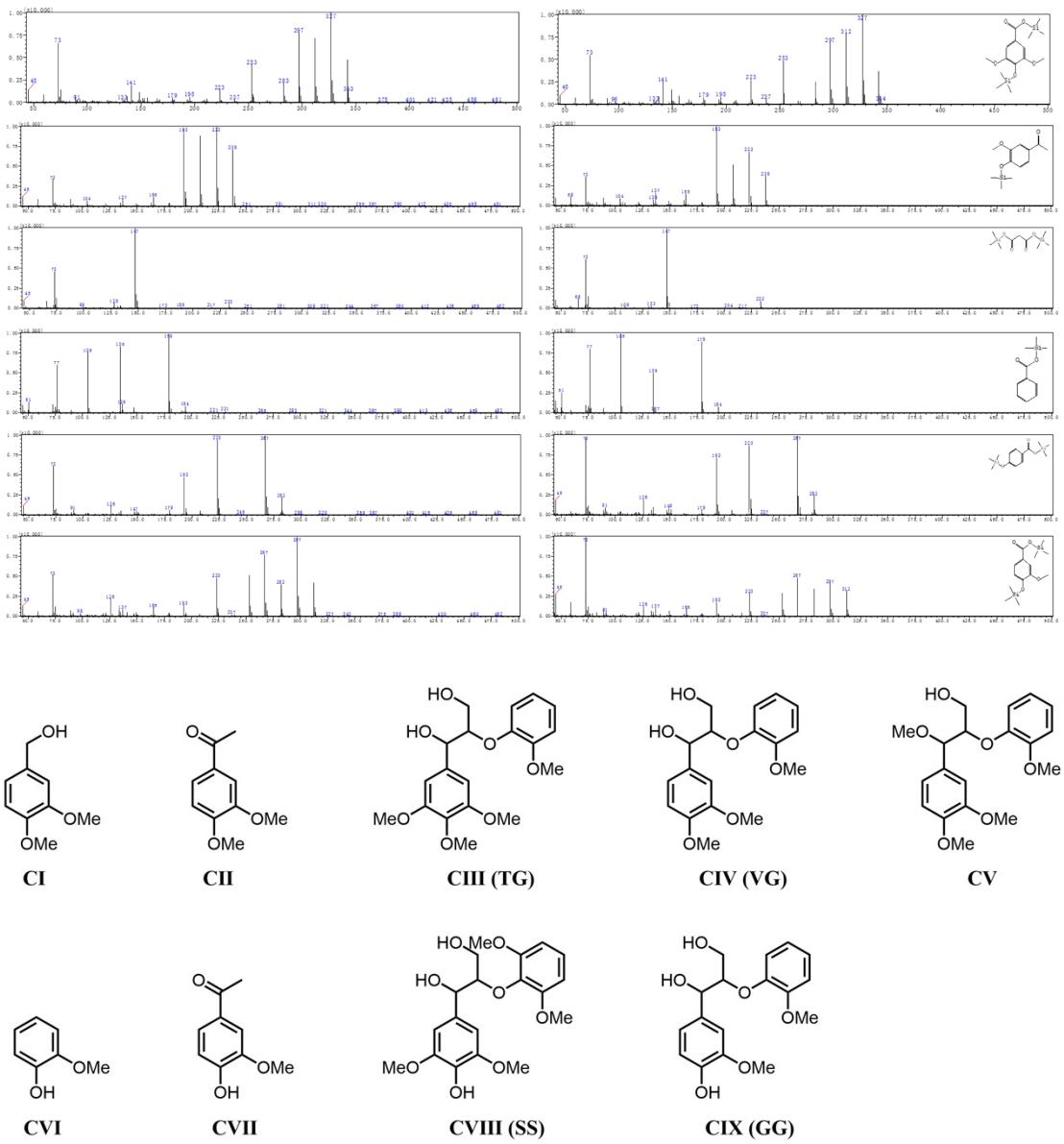

Fig. S21 Types of lignin models.

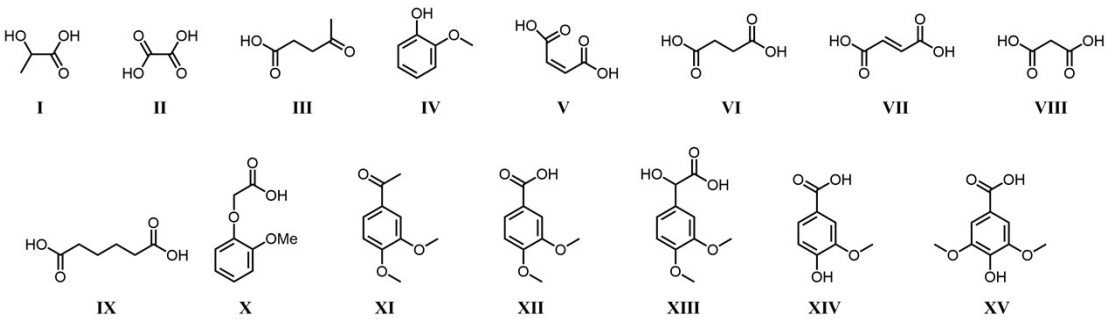

Fig. S22 Types of electrocatalytic degradation products.

Table S1 Summary of degradation results of non-phenolic lignin models.

Non-phenolic substrate	Time (h)	Product yield (%)													Yield A (%)	Yield B (%)	Conv. (%)
		I	II	III	IV	V	VI	VII	IX	X	XI	XII	XIII	VG			
CI	3											80.0				80	95
CII	9											44.4				44	57
CIII	9	0.5	7.8	0.3		1.1	1.4	4.7	1.8	2.8		92.0			20	92	100
CIV	9	0.6	6.3			0.4	2.4	1.7	6.3	2.8	1.0	92.7	0.6		20	94	100
CV	9											8.3		14.5		23	30

Table S2 Summary of degradation results of phenolic lignin models.

Phenolic substrate	Time (h)	Product yield (%)												Yield (%)	Conv. (%)
		I	II	III	IV	V	VI	VII	XV	VIII	IX	X	XIV		
CVI	6	0.7	3.8		0.3	0.1	0.3	0.3		0.2	1.3			6	100
CVII	6	1.5	12.3	0.3		0.2	0.6	0.5		0.2	2.5			17	99
CVIII	9	1.4	36.3	0.5		0.2	4.3	1.1	1.1		0.3			45	94
CIX	9	0.3	8.0	0.3	1.6	2.4	1.3	2.0		0.4	3.5	2.1	0.8	23	99

Computational method

The study used VASP to perform density functional theory calculations with projector augmented wave. Electron spin polarization were considered in all calculations. The Perdew-Burke-Ernzerhof functional was employed for exchange-correlation effects, while DFT+D3 was used for handling weak interactions. The cut-off energy for the plane-wave basis was 450 eV. K-points were 2*2*1 in the Brillouin zone. 15 Å of layer vacuum was applied at Z-axis of slab models to avoid the Periodic effect. Energy and maximum stress were converged to 10^{-5} eV and 0.02 eV/Å, respectively.

Fig. S23 The ^{1}H-NMR and ^{13}C-NMR of the synthesized models .

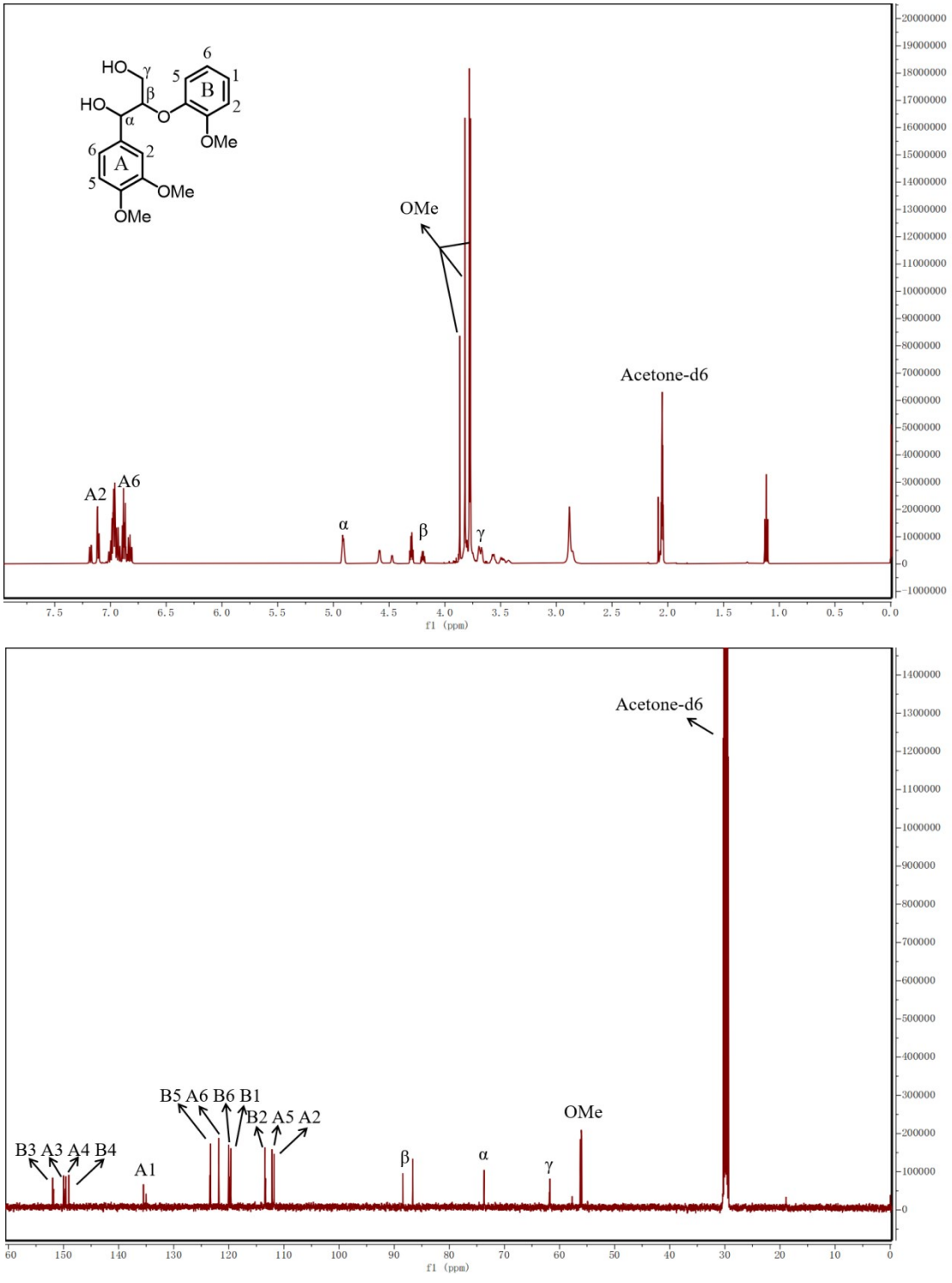

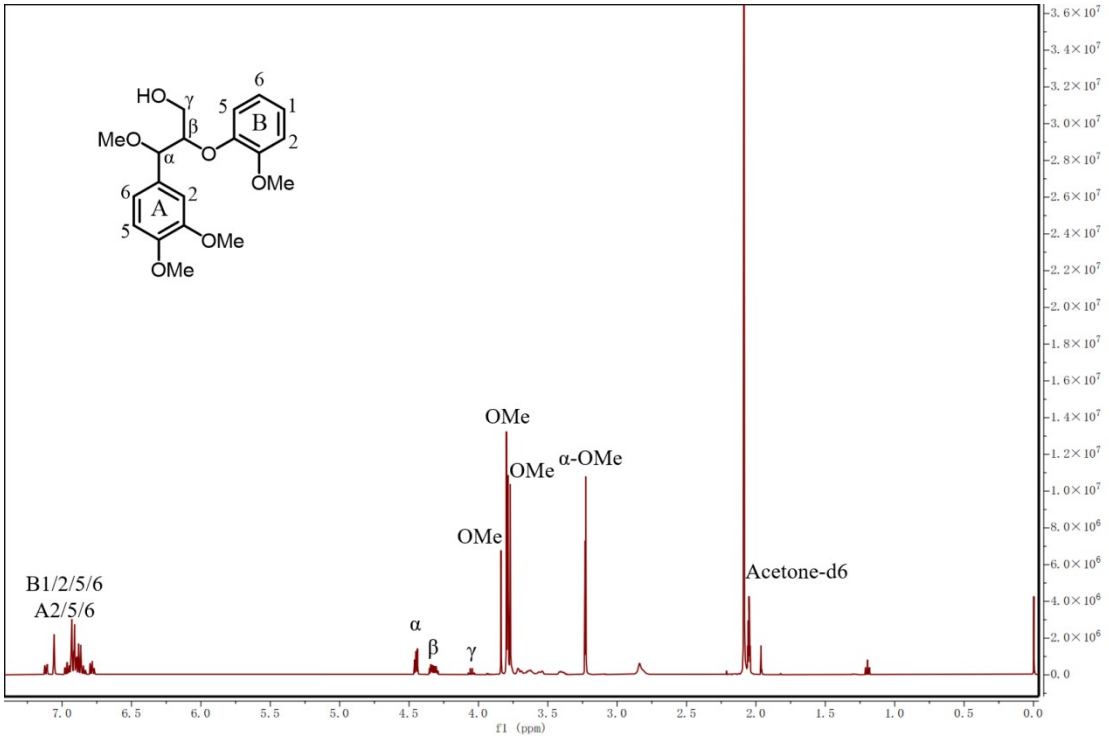
HO
γ
β
α
MeO
O
OMe
OMe
OMe
A
B
1
2
5
6
B1/2/5/6
A2/5/6
α
β
γ
OMe
OMe
α-OMe
OMe
Acetone-d6
f1 (ppm)

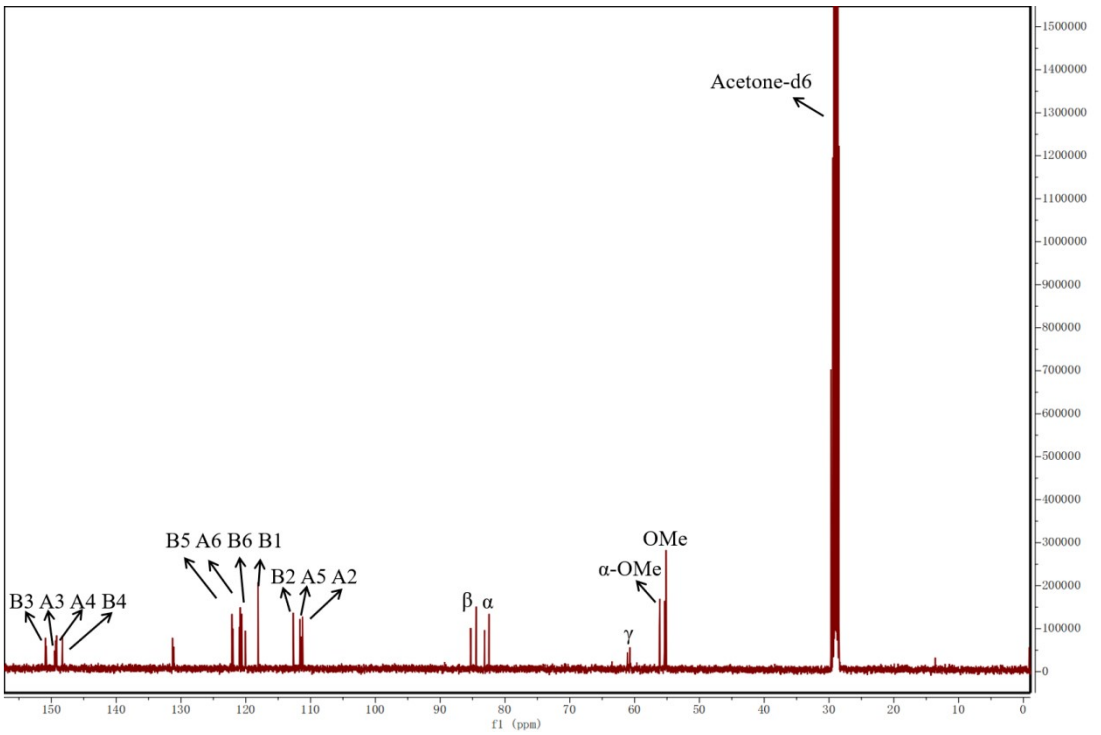
Acetone-d6
B5 A6 B6 B1
B2 A5 A2
B3 A3 A4 B4
β α
γ
α-OMe
OMe
f1 (ppm)

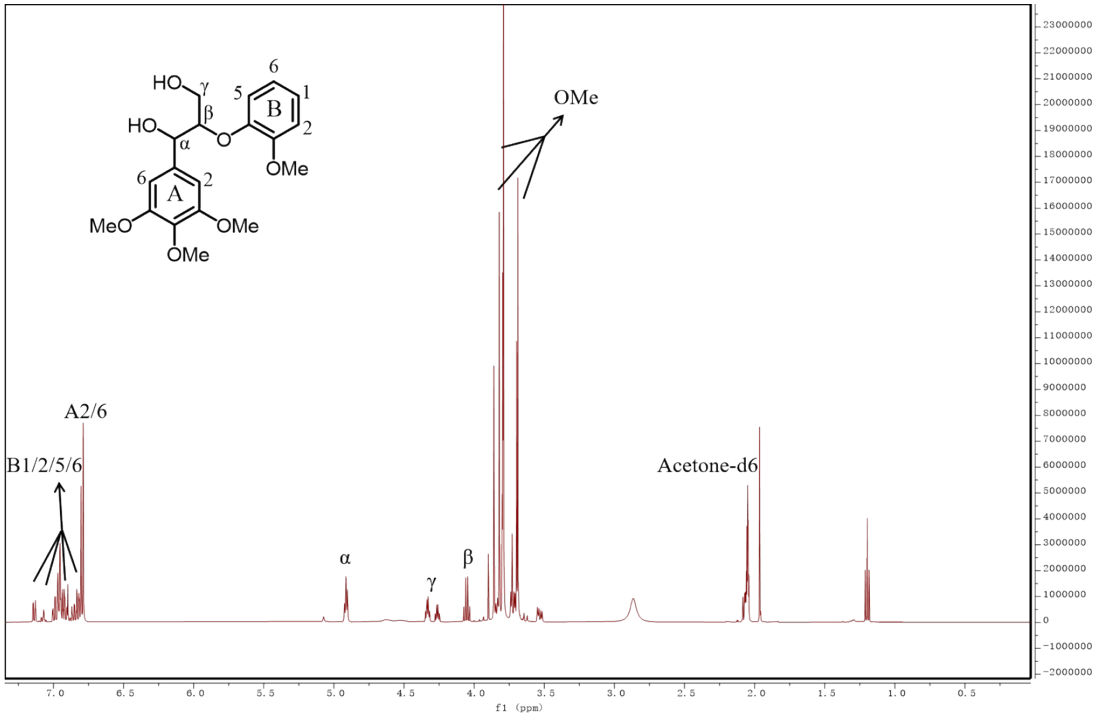
HO
γ
β
α
HO
O
6
5
B
1
2
OMe
6
A
2
MeO
OMe
OMe
OMe
A2/6
B1/2/5/6
α
γ
β
Acetone-d6
f1 (ppm)

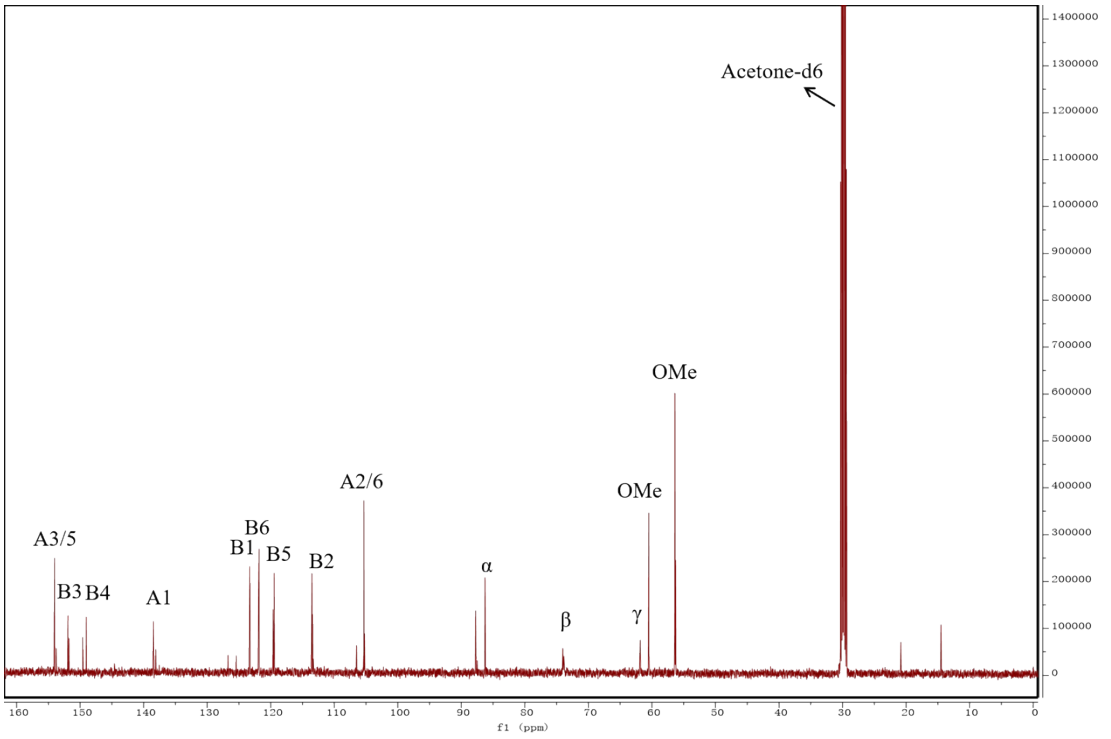
Acetone-d6
OMe
OMe
A2/6
A3/5
B6
B1
B5
B2
α
B3 B4
A1
β
γ
f1 (ppm)

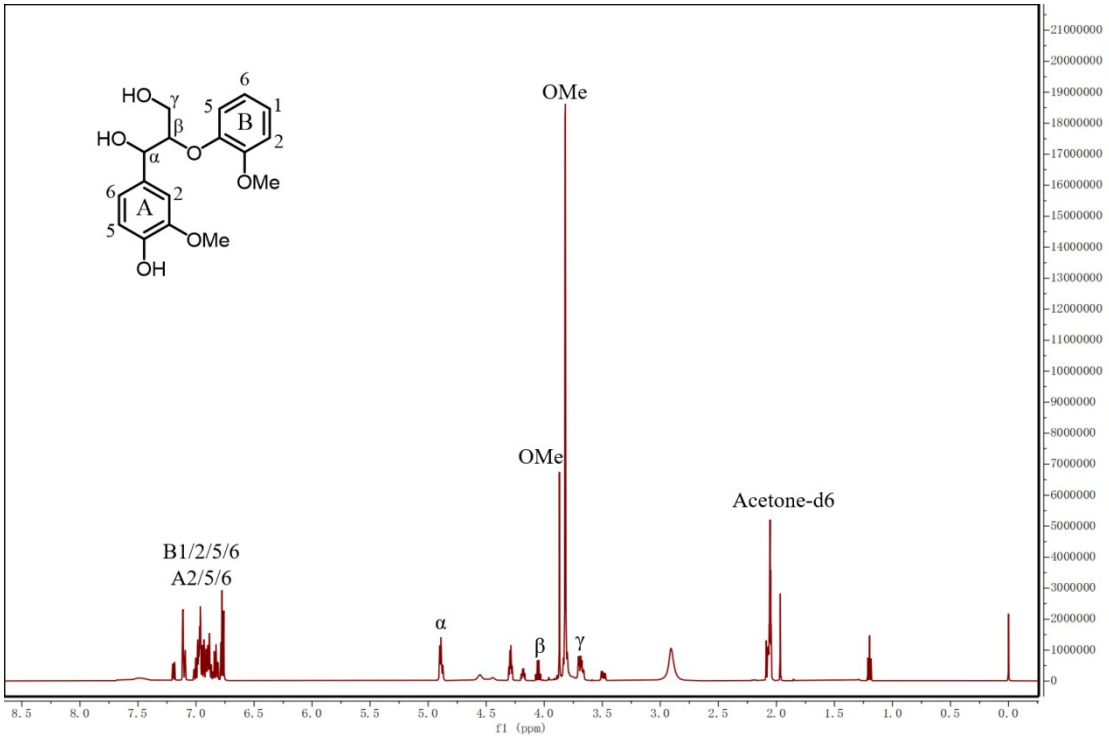
HO
γ
β
α
HO
O
6
5
B
1
2
OMe
6
A
2
5
OMe
OH
OMe
OMe
Acetone-d6
B1/2/5/6
A2/5/6
α
β
γ
f1 (ppm)

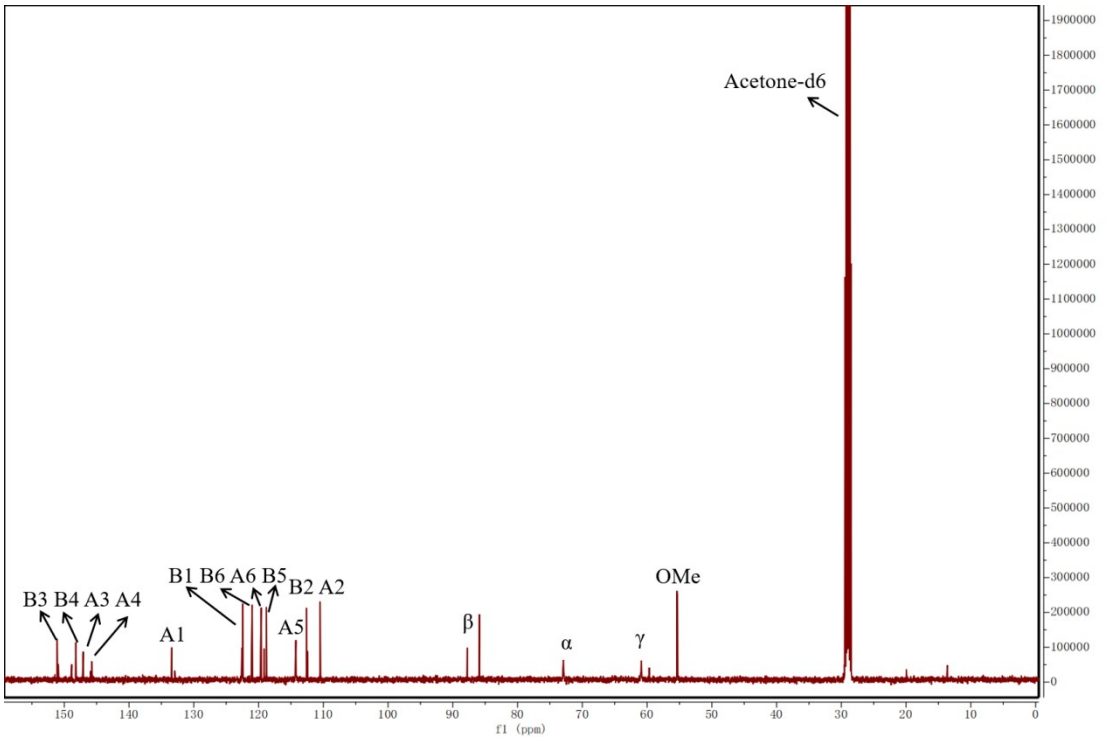
Acetone-d6
B3 B4 A3 A4
B1 B6 A6 B5
B2 A2
A1
A5
β
α
γ
OMe
f1 (ppm)

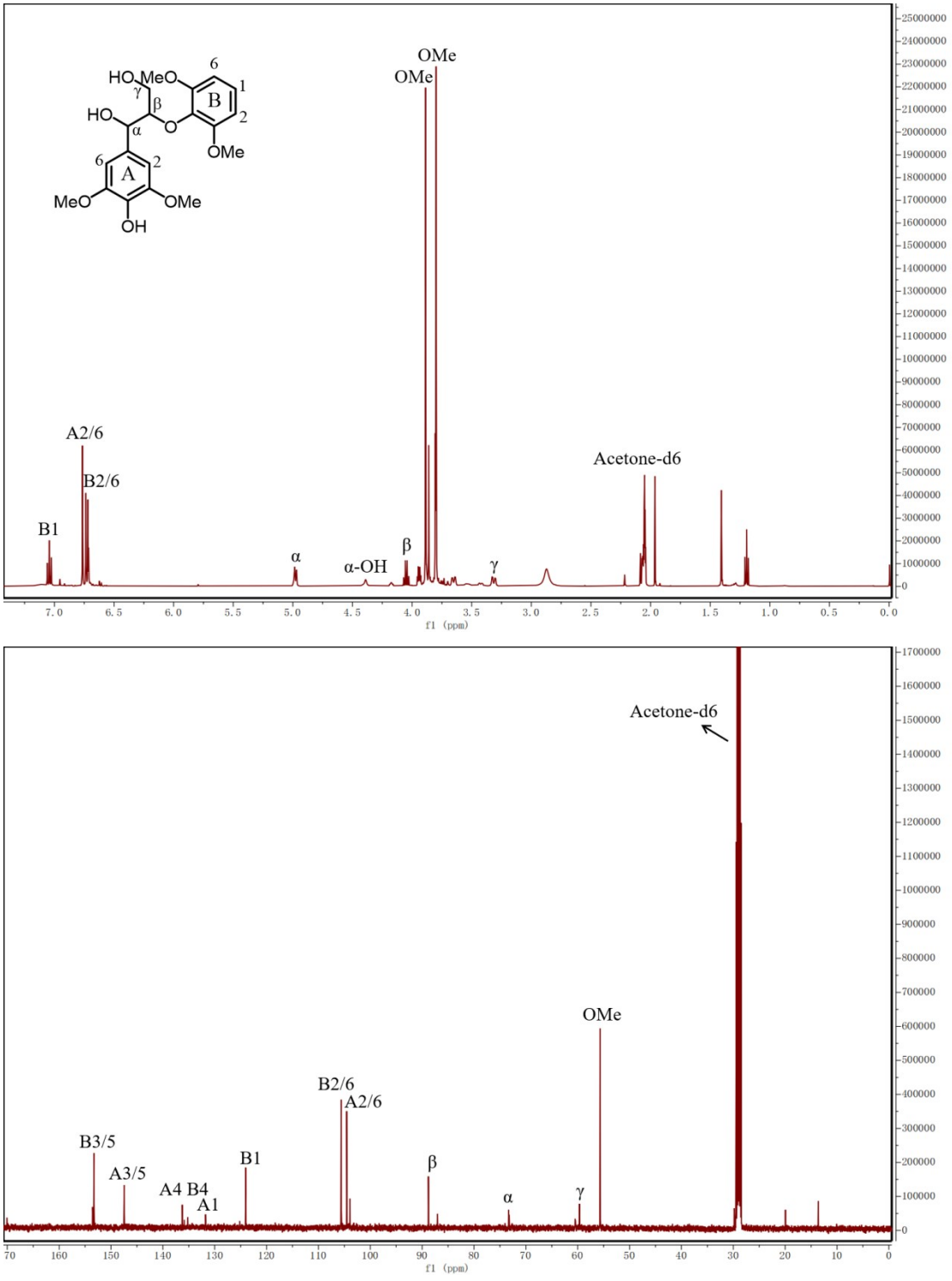

1. S. Kawai, K. Okita, K. Sugishita, A. Tanaka and H. Ohash, *Journal of wood science*, 1999, **45**, 440-443.